7 Stator Magnetic Design

This chapter investigates the magnetic field distribution within the stator. This magnetic field is due to two sources—the magnetic field crossing the air gap from the rotor, and the magnetic field created by currents flowing in the stator windings. Of these, the magnetic field entering the stator from the rotor dominates the magnetic field created by winding currents. Moreover, the magnetic field crossing the air gap from the rotor determines the mutual torque created by the motor.

The magnetic field distribution given in (6.1) describes the air gap flux density entering the stator under the assumption that there are no stator slots. When computing the magnetic flux entering and flowing through the stator teeth, the influence of the stator slots must be taken into account. Because the stator slots are fixed to the stator and the air gap magnetic field rotates with the rotor, the impact of the stator slots varies with rotor position.

In addition, the magnetic field described in (6.1) assumes that the ferromagnetic material in the rotor yoke and stator is infinitely permeable. The actual finite relative permeability of the ferromagnetic material has little effect on the spatial variation of the magnetic field distribution. The primary error introduced by this assumption is an implied zero MMF across the ferromagnetic portions of the motor. This assumption makes the amplitude of the air gap flux density distribution too large. As with the presence of slots, the effect of finite ferromagnetic material permeability will be taken into account by modifying the magnetic field distribution determined under the ideal conditions.

Before considering stator magnetic design details, it is beneficial to consider what is known about the air gap magnetic field as given by (6.1). As defined in Chapter 6, the magnetic field exhibits half wave symmetry for all common rotor constructions because the magnetic field over South and North magnetic poles differ by only their flux direction. As a result, all even harmonics in (6.1) are zero. In addition, given that $\theta = 0$ was defined at the center of a North magnet pole, the air gap flux density exhibits even symmetry, making all of its Fourier series coefficients real.

7.1 Influence of Stator Slots

The presence of slots changes or perturbs the magnetic field in the air gap in the vicinity of the slots, with the perturbation varying as a function of the size of the slot opening and the air gap length. In addition, this perturbation is also a function

of the saturation of the ferromagnetic materials used in the rotor and stator. In particular, the saturation of the shoe tips influences the amplitude and distribution of the perturbation. Since this effect is impossible to describe analytically, it must be ignored. However, it does point to the desirability of making the shoe radial depth sufficiently large to minimize shoe tip saturation. This fact calls for a compromise, since it is in conflict with maximizing the slot area available for windings.

A number of techniques for describing the magnetic field perturbation due to stator slots appear in the literature. Some parameterize the perturbation throughout the air gap and magnet regions. Some accommodate shoe tip saturation by making the perturbation apply to an empirically-determined area wider than the slot opening. In brushless permanent magnet motor design, the radial magnetic field entering the stator determines the flux linkage, back EMF, and mutual torque. As a result, the influence of stator slots need only be considered at the stator surface.

The fundamental principle governing the influence of the stator slots is the fact that the magnetic field over the slots must travel further to reach the stator ferromagnetic material as shown in **Fig. 7-1**. Simply put, the air gap length is larger over the slots. Because of the larger effective air gap, the flux density is reduced over the slot region. This fact is easily understood by considering the surface permanent magnet rotor case as analyzed in Chapter 4. Substituting (2.33) into (4.4), the air gap flux density can be written as

$$B_g = \frac{K_l C_\phi}{1 + K_r \dfrac{\mu_R g}{l_m} C_\phi} B_r \tag{7.1}$$

This expression describes the amplitude of the air gap flux density in an idealized motor structure as a function of the magnet material and geometrical parameters.

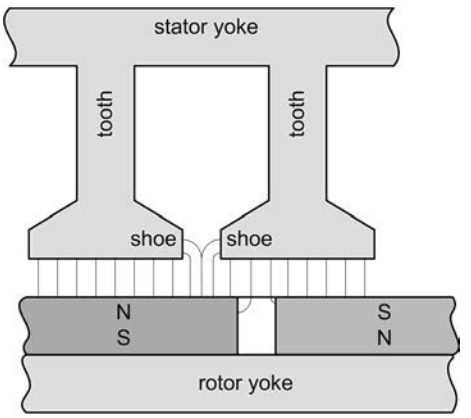

Figure 7-1. Representative permanent magnet flux flow pattern.

With all other parameters fixed, an increase in the air gap length g in (7.1) causes the air gap flux density B_g to decrease.

Equation (7.1) provides a simple heuristic way to approximate the influence of slots on the radial magnetic field entering the stator. Let (7.1) describe the ideal flux density in the absence of slots where g is the nominal air gap length, and let

$$B_g(\theta_{st}) = \frac{K_l C_\phi}{1 + K_r \dfrac{\mu_R g(\theta_{st})}{l_m} C_\phi} B_r \tag{7.2}$$

describe the flux density as the air gap length varies as described by $g(\theta_{st})$, where position θ_{st} is angle with respect to a stator tooth. Then, the ratio of (7.2) to (7.1) describes a slot correction factor that can be applied to the ideal magnetic field distribution at the stator surface $B_{gs}(\theta_e)$ to accommodate for the influence of stator slots. In the literature, this correction factor is commonly called a relative permeance. Therefore, the air gap flux density entering the stator teeth in the presence of stator slots can be written as

$$B_{gt}(\theta_e) = K_{sl}(\theta_{st}) B_{gs}(\theta_e) \tag{7.3}$$

where $K_{sl}(\theta_{st})$ is the slot correction factor, θ_{st} is angle with respect to the stator coordinate system, $B_{gs}(\theta_e)$ is given by (6.1) in which θ_e is electrical angle with respect to the center of a North magnetic pole on the rotor. Taking the ratio of (7.2) to (7.1), the slot correction factor for motors having surface magnet rotors can be written as

$$K_{sl}(\theta_{st}) = \frac{B_g(\theta_{st})}{B_g} = \frac{\dfrac{l_m}{g} + K_r \mu_R C_\phi}{\dfrac{l_m}{g} + K_r \mu_R C_\phi \dfrac{g(\theta_{st})}{g}} \tag{7.4}$$

Because this is an approximation and because $K_r \mu_R C_\phi \approx 1$ and $K_r \mu_R C_\phi < l_m/g$, (7.4) can be rewritten with sufficient accuracy as

$$K_{sl}(\theta_{st}) = \frac{1 + \dfrac{l_m}{g}}{\dfrac{g(\theta_{st})}{g} + \dfrac{l_m}{g}} \tag{7.5}$$

As the rotor passes by stator slots, the relative permeance or slot correction factor $K_{sl}(\theta_{st})$ modifies the air gap flux density in the neighborhood of the stator slots. When over a stator tooth, $g(\theta_{st})$ is equal to g, and the relative permeance (7.5) is equal to one as expected. When over the center of a slot, $g(\theta_{st}) > g$, and the slot cor-

rection factor becomes less than one, which decreases the flux density entering the tooth relative to the air gap flux density according to (7.3).

To complete this analysis, the variation in the air gap length $g(\theta_{st})$ must be specified in the slot area. The most rudimentary solution is to assume that $g(\theta_{st})$ is infinitely large over the slots. This assumption makes the air gap flux density over the slots equal to zero. A better solution is to use the circular-arc, straight-line flux flow approximation as described in Chapter 2 and depicted in Fig. 2-9. In doing so, $g(\theta_{st}) = g + (\pi/2)x$ where x is the linear distance into the slot area from a tooth edge. Applying this approach and using the geometry shown in **Fig. 7-2** results in the normalized air gap length over the range $-\theta_{sp}/2 = \theta_{st} = \theta_{sp}/2$ being

$$\frac{g(\theta_{st})}{g} = \begin{cases} 1 & |\theta_{st}| \le \theta_t/2 \\ 1+\dfrac{\pi}{2}\dfrac{R_{si}}{g}\left(\theta_{st}-\theta_t/2\right) & \theta_t/2 \le \theta_{st} \le \theta_{sp}/2 \\ 1-\dfrac{\pi}{2}\dfrac{R_{si}}{g}\left(\theta_{st}+\theta_t/2\right) & -\theta_{sp}/2 \le \theta_{st} \le -\theta_t/2 \end{cases} \tag{7.6}$$

where all angles are in mechanical measure on the stator.

The slot correction factor model that results when (7.6) is substituted into (7.5) assumes that the flux density is unchanged over the entire surface of the tooth at the air gap. In reality, the flux density begins to decrease as one nears the slot opening. In addition, this modeling makes the change in flux density more abrupt and less smooth than occurs in practice. To better approximate the actual flux density distribution over a slot, it is common to initiate slot correction over the tooth starting $0.3\theta_{so}$ from the slot edge and to let the slot correction factor have a sinusoidal shape over the slot opening.

Evaluating (7.6) at the slot centerline and substituting this value into (7.5) gives the minimum value of the slot correction factor as

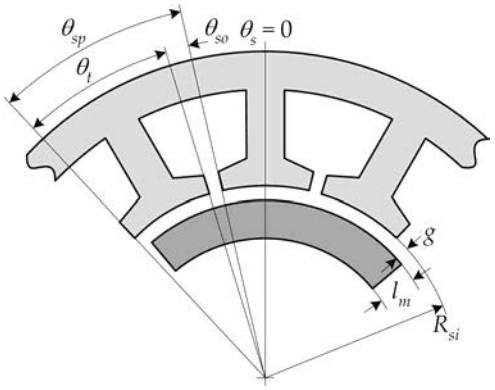

Figure 7-2. Geometry for the computation of the slot correction factor.

$$K_{sbm} = \frac{1 + \frac{l_m}{g}}{1 + \frac{l_m}{g} + \frac{\pi R_{si} \theta_{so}}{4g}} \tag{7.7}$$

Using this slot correction value at the slot centerline and a value of one at $0.8\theta_{so}$ away from the slot centerline as two fitting points for a sinusoidal shape, the resulting improved slot correction factor becomes

$$K_{sl}(\theta_{st}) = \begin{cases} 1 & |\theta_{st}| \le \theta_{tr} \\ \frac{1+K_{sbm}}{2} + \frac{1-K_{sbm}}{2} \cos\left(\frac{\pi\left(|\theta_{st}| - \theta_{tr}\right)}{0.8\theta_{so}} \right) & \theta_{tr} \le |\theta_{st}| \le \theta_{sp}/2 \end{cases} \tag{7.8}$$

where θ_{tr} is the transition angle $\theta_{tr} = \theta_{sp}/2 - 0.8\theta_{so}$.

To illustrate the slot correction factor, **Fig. 7-3** shows the two slot correction factors considered here using typical parameter values. In the figure, the vertical dotted lines mark the tooth edges and slot centerlines, the dashed line depicts the initial approximation given by the substitution of (7.6) into (7.5), and the solid line illustrates the improved slot correction factor given by (7.8).

The slot correction factor considered here applies to the surface permanent magnet rotor case. For the spoke magnet rotor case, the slot correction factor can be

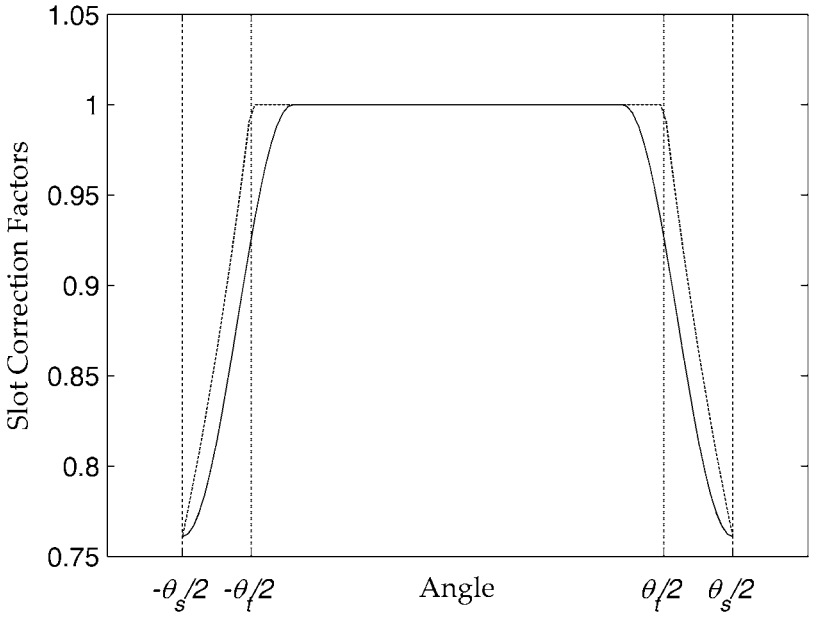

Figure 7-3. Slot correction factor illustration.

found by using the air gap flux density expression (6.6) rather than (7.1). Similarly, the buried magnet case can be considered by using the air gap flux density expression (6.9) rather than (7.1).

7.2 Tooth Flux

The next chapter demonstrates that all coils in a motor can be described in terms of a sequence of equivalent single tooth coils. For example, consider the coil and its single tooth equivalent shown in **Fig. 7-4**. If $\phi_1(\theta_e)$ describes the flux in the first tooth as a function of the rotor position θ_e in electrical measure, then the flux in the second tooth is $\phi_2(\theta_e) = \phi_1(\theta_e - \theta_{spe})$ where θ_{spe} is the angular slot pitch or period in electrical measure. Similarly, $\phi_3(\theta_e) = \phi_1(\theta_e - 2\theta_{spe})$ is the flux in the third tooth making up the coil. Then the flux linking the coil on the left in the figure is described by $\phi_c(\theta_e) = \phi_1(\theta_e) + \phi_1(\theta_e - \theta_{spe}) + \phi_1(\theta_e - 2\theta_{spe})$.

As described above, the tooth flux plays a crucial role in determining motor performance. From basic principles, this flux is given by the integral of the flux density over one slot pitch and axial motor length as

$$\phi = \int \vec{B} \cdot \vec{dA}$$

Application of this integral to the geometry shown in **Fig. 7-5** gives the tooth flux as

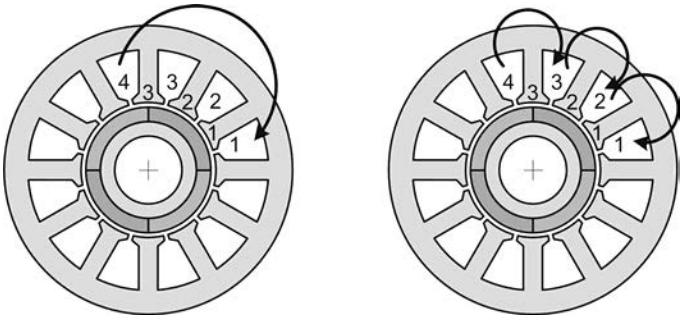

Figure 7-4. A coil and its single tooth equivalent.

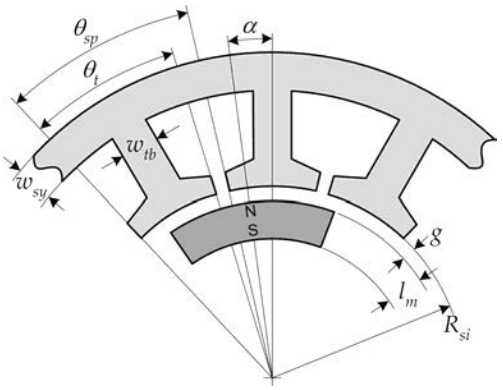

Figure 7-5. Geometry for the computation of tooth flux.